# Impact of Asian emissions on observations at Trinidad Head, California, during ITCT 2K2

Allen H. Goldstein,[1] Dylan B. Millet,[1] Megan McKay,[1] Lyatt Jaeglé,[2] Larry Horowitz,[3] Owen Cooper,[4,5] Rynda Hudman,[6] Daniel J. Jacob,[6] Sam Oltmans,[5] and Andrew Clarke[5]

Received 1 December 2003; revised 18 February 2004; accepted 19 March 2004; published 9 July 2004.

[1] Field measurements of a wide suite of trace gases and aerosols were carried out during April and May 2002, along with extensive chemical transport modeling, as part of the NOAA Intercontinental Transport and Chemical Transformation study. Here, we use a combination of in-situ ground-based measurements from Trinidad Head, CA, chemical transport modeling, and backward trajectory analysis to examine the impact of long-range transport from Asia on the composition of air masses arriving at the California coast at the surface. The impact of Asian emissions is explored in terms of both episodic enhancements and contribution to background concentrations. We find that variability in CO concentrations at the ground site was largely driven by North American emissions, and that individual Asian plumes did not cause any observable pollution enhancement episodes at Trinidad Head. Despite this, model simulations suggest that Asian emissions were responsible for 33% of the CO observed at Trinidad Head, providing a larger mean contribution than direct emissions from any other region of the globe. Surface ozone levels were found to depend primarily on local atmospheric mixing, with surface deposition leading to low concentrations under stagnant conditions. Model simulations suggested that on average 4 ± 1 ppb of ozone (10% of observed) at Trinidad Head was transported from Asia. *INDEX TERMS:* 0322 Atmospheric Composition and Structure: Constituent sources and sinks; 0345 Atmospheric Composition and Structure: Pollution—urban and regional (0305); 0365 Atmospheric Composition and Structure: Troposphere—composition and chemistry; 0368 Atmospheric Composition and Structure: Troposphere—constituent transport and chemistry; 1610 Global Change: Atmosphere (0315, 0325); *KEYWORDS:* Asian emission, carbon monoxide, ozone

**Citation:** Goldstein, A. H., D. B. Millet, M. McKay, L. Jaeglé, L. Horowitz, O. Cooper, R. Hudman, D. J. Jacob, S. Oltmans, and A. Clarke (2004), Impact of Asian emissions on observations at Trinidad Head, California, during ITCT 2K2, *J. Geophys. Res.*, *109*, D23S17, doi:10.1029/2003JD004406.

## 1. Introduction

[2] Modeling and measurement studies have demonstrated that large-scale transport of continental emissions in the highly industrialized northern midlatititudes can significantly affect air quality and chemistry thousands of kilometers downwind [e.g., *Penkett et al.*, 1998; *Hoell et al.*, 1997; *Parrish et al.*, 1993; *Wild and Akimoto*, 2001]. East Asia is a strong and growing source region for pollutants such as carbon monoxide, aerosols, and ozone precursor species including volatile organic compounds (VOCs) and oxides of nitrogen. The extent to which these emissions impact atmospheric composition in North America has important ramifications both in terms of enhancing high pollution episodes and by defining the "background" concentrations that set the lower limits on what can be achieved by U.S. and California air quality regulations.

[3] Ground, airborne, and satellite based measurements of suites of chemical compounds combined with backward trajectory analyses have been used over the past two decades to document approximately 20 plumes of air pollution from Asia reaching the west coast of North America [*Andreae et al.*, 1988; *Kritz et al.*, 1988; *Parrish et al.*, 1992; *Jaffe et al.*, 1999; *Jaffe et al.*, 2003a; *Husar et al.*, 2001; *McKendry et al.*, 2001; *Thulasiraman et al.*, 2002; *VanCuren and Cahill*, 2002; *Jaeglé et al.*, 2003, *Forster et al.*, 2004; *Cooper et al.*, 2004], providing clear experimental evidence that this pollution indeed reaches the western United States. These studies used a range of compounds including radon (Rn), particle composition, CO, $O_3$, and VOCs to provide evidence of the transport events. The observed events were highly episodic, with the

[1]Department of Environmental Science, Policy, and Management, University of California, Berkeley, California, USA.
[2]Department of Atmospheric Science, University of Washington, Seattle, Washington, USA.
[3]National Oceanic and Atmospheric Administration, Geophysical Fluid Dynamics Laboratory, Princeton, New Jersey, USA.
[4]Cooperative Institute for Research in Environmental Sciences, University of Colorado, Boulder, Colorado, USA.
[5]National Oceanic and Atmospheric Administration, Aeronomy Laboratory, Boulder, Colorado, USA.
[6]Division of Engineering and Applied Sciences and Department of Earth and Planetary Sciences, Harvard University, Cambridge, Massachusetts, USA.


0148-0227/04/2003JD004406$09.00

vast majority occurring in springtime. This is when trans-Pacific transport is thought to be most efficient due to prefrontal flow lofting pollutants from the surface followed by southeastward moving cold fronts which transport the pollutants above the boundary layer [*Liu et al.*, 2003; *Forster et al.*, 2004]. The majority of these events were not observed at ground-based stations, but rather at higher elevations using aircraft measurements. $O_3$ levels were not typically enhanced during the Asian transport periods, but particles, CO, Rn and/or VOCs were.

[4] Several recent modeling studies have focused on estimating Asian emission impacts on North American air quality. *Jacob et al.* [1999] coupled the Harvard-GISS global 3D tropospheric chemistry model with projected increases in Asian anthropogenic emissions. They forecasted that the expected tripling of Asian emissions from 1985–2010 would result in an increase in monthly mean surface ozone of 2–6 ppb in the western U.S. and 1–3 ppb in the eastern U.S. Their model results suggested that in the western U.S., this would negate the benefits of a hypothetical 25% reduction in $NO_x$ and VOC emissions. In another modeling study, *Berntsen et al.* [1999] calculated the present-day Asian contribution to background CO, peroxyacetylnitrate (PAN), and $O_3$ in air reaching the west coast of the U.S. Average background enhancements during spring due to Asian anthropogenic emissions were estimated to be 34 ppb, 26 ppt, and 4 ppb for CO, PAN and $O_3$. Maximum enhancements in these species during simulated episodic pollution incursions from Asia were 42 ppb, 75 ppt, and 7.5 ppb, respectively. While outflow of Asian emissions acted to elevate both background and maxima for CO and PAN concentrations in the western U.S., the impact on $O_3$ was to increase average concentrations but not to exacerbate maximum ozone levels during pollution events. Presumably this is because conditions leading to effective trans-Pacific transport of pollutants are anticorrelated with conditions leading to high local ozone levels.

[5] Most of the observations and analysis of Asian pollution transport to North America have focused on specific events when coherent plumes were observed [e.g., *Jaffe et al.*, 2003a]. Although modeling studies have shown that the transport of pollution from Asia is a pervasive and persistent phenomena [e.g., *Jaeglé et al.*, 2003], only recently has observational evidence been used to make this point. *VanCuren and Cahill* [2002] and *Van Curen* [2003] showed that Asian dust is a regular component of the aerosol over western North America, and is commonly observed across the North American continent, with maximum concentrations observed at sites at least 500 m above sea level.

[6] The NOAA Intercontinental Transport and Chemical Transformation 2002 (ITCT 2K2) study was carried out in the spring of 2002, with the primary goal of better quantifying the transport of pollution, in particular CO, ozone and its precursors, fine particles, and other chemically and radiatively active compounds, into North America. The overall study involved ground-based measurements at two sites on the west coast of the United States, and airborne measurements aboard aircraft flying east-west across the Pacific and north-south along the west coast of the United States. In addition, several modeling teams generated pollution forecasts multiple times daily for use in flight and scientific planning. These observational and modeling efforts are fully described in this special issue of the *Journal of Geophysical Research*. As part of ITCT 2K2, NOAA established a ground site at Trinidad Head, on the northern California coast, equipped with instrumentation for in-situ measurement of a wide variety of trace gas species, aerosol composition and physical properties, and supporting meteorological data. This paper focuses on analyzing the CO and $O_3$ observations from Trinidad Head, and comparing observations with results from two independent model simulations and a backward trajectory model, with the goal of understanding what controls the composition of air masses entering North America in springtime at the ground. We separate the analysis to distinguish between contributions to plumes versus contributions to the persistent background concentrations in order to determine: (1) Were Asian plumes identifiable? (2) What were the total contributions of different sources to observed mixing ratios?

## 2. Experiment

### 2.1. Field Site

[7] The ITCT ground-based field measurement station was installed at Trinidad Head, on the northern coast of California (41.054°N, 124.151°W, 107 m elevation), and was operative from 19 April–22 May 2002. Instrumentation was housed in two climate-controlled laboratory containers. Sampling inlets were mounted atop a 10 m scaffolding tower between the laboratory containers.

### 2.2. Measurements

[8] Volatile organic compounds were measured using a fully automated, in-situ GC/MSD/FID system that is described in detail elsewhere [*Millet et al.*, 2004]. For 36 minutes out of every hour, two subsample flows (15 sccm) were drawn from the main sample line (4 slm) and passed through a preconditioning trap for the removal of water (−25°C cold trap). Carbon dioxide and ozone were then removed from the FID channel subsample (Ascarite II), and ozone was removed from the MSD channel subsample (KI impregnated glass wool). Preconcentration was accomplished using a combination of thermoelectric cooling (−15°C) and adsorbent trapping. Samples were injected into the GC by rapidly heating the trap assemblies to 200°C. The instrument was calibrated several times daily by dynamic dilution of low ppm level standards (Scott Marrin Inc., and Apel-Riemer Environmental Inc.) into zero air to achieve near ambient concentrations. Zero air was analyzed daily to check for blank problems and contamination for all measured compounds. For methyl-t-butyl-ether, the measurement precision (defined as the relative standard deviation of the calibration fit residuals) and the limit of detection were 1.2% and 0.4 ppt, respectively. We estimate the absolute accuracy at better than ±10%.

[9] CO was measured by gas filter correlation, nondispersive infrared absorption (TEI 48C). Ozone was measured using a UV photometric $O_3$ analyzer (Dasibi 1008-RS), and $CO_2$ by infrared absorption using a LI-6262 (Li-Cor Inc.). Incoming photosynthetically active radation (PAR) was measured with LI-190SZ Quantum Sensor (Li-Cor Inc.). Wind speed and direction were monitored with a propeller wind monitor (R.M. Young Co.) mounted on a 3 m tower on

top of the laboratory container, and ambient air temperature was measured using an HMP45C Temperature and RH probe (Campbell Scientific Inc.).

[10] Additional gas phase measurements made at the site (not reported here) included $NO/NO_y$ by $NO\text{-}O_3$ chemiluminescence and $^{222}Rn$ using a dual-flow loop, two-filter radon detector [*Whittlestone and Zahorowski*, 1998]. Time resolved aerosol measurements at the site (not reported here) included chemical composition using an Aerodyne aerosol mass spectrometer (AMS, Aerodyne Research Inc.) [*Jimenez et al.*, 2003; *Allan et al.*, 2003] and a particle-into-liquid sampler (PILS) [*Weber et al.*, 2001; *Orsini et al.*, 2003], number density (7 nm–2.5 μm) using a condensation particle counter (CPC, model 3022a, TSI Inc.), and elemental composition using an 8-stage drum impactor and synchrotron X-Ray fluorescence [*Bench et al.*, 2002; *Cahill and Wakabayashi*, 1993; *Perry et al.*, 1999].

[11] Balloon sondes launched daily from the site measured ozone concentrations and meteorological parameters with 1.2 second resolution from the surface to approximately 35 km elevation.

### 2.3. Chemical Transport and Trajectory Models

#### 2.3.1. GEOS-CHEM

[12] The GEOS-CHEM global chemical transport model [*Bey et al.*, 2001a] is driven by assimilated meteorological data from the NASA Goddard Earth Observing System (GEOS) Global Modeling Assimilation Office (GMAO). In this study, we used version 5.03 of GEOS-CHEM (http://www-as.harvard.edu/chemistry/trop/geos) with a horizontal resolution of 2° latitude by 2.5° longitude and 30 vertical levels. The CO emission inventory includes fossil fuel [*Bey et al.*, 2001a], biofuel [*Yevich and Logan*, 2003] and climatological biomass burning [*Duncan et al.*, 2003] emissions. Over Asia (10S–60N; 60–150E) our annual CO emissions are: 165 Tg/yr (fossil fuel), 90 Tg/yr (biofuel), and 120 Tg/yr (biomass burning).

[13] Individual source regions are tagged in order to resolve the origin of CO and ozone. For the tagged CO simulation, we use separate tracers to track Asian emissions from anthropogenic emissions (including both fossil fuel and biofuel sources), biomass burning emissions, as well as anthropogenic emissions from North America, and Europe. Here we define the respective regions as: Asia (12S–88N; 65–153E), N. America (24–88N; 142–48W), and Europe (36–88N; 18W–65E).

[14] We present results for a full $O_3\text{-}NO_x$-hydrocarbon simulation as well as a CO-only simulation using monthly OH fields from the full chemistry simulation as described in previous studies [*Bey et al.*, 2001b; *Liu et al.*, 2003; *Jaeglé et al.*, 2003] and an $O_3$-only simulation using archived daily ozone production rates and loss frequencies [*Li et al.*, 2002; *Liu et al.*, 2002]. The tagged ozone simulation tracks the transport of ozone produced from precursor emissions in the lower troposphere over Asia, Europe and North America [*Jaeglé et al.*, 2003].

#### 2.3.2. MOZART-2

[15] MOZART-2 (Model of Ozone And Related chemical Tracers, version 2) is a global chemical transport model designed to simulate the distribution of tropospheric ozone and its precursors [*Horowitz et al.*, 2003]. MOZART-2 simulates the concentrations of 63 chemical species from the surface up to the middle stratosphere. In this study, the model is driven with meteorological inputs from the NCEP Aviation (AVN) model analyses, which have a resolution of T170 (approximately 0.7° latitude × 0.7° longitude) with 42 vertical levels extending up to 2 hPa. The meteorological fields are averaged to a horizontal resolution of 1.9° latitude × 1.9° longitude, the resolution at which MOZART-2 is run. A time step of 15 minutes is used for all chemistry and transport processes.

[16] Meteorological parameters, including zonal and meridional winds, temperature, specific humidity, surface pressure, and surface fluxes of heat and momentum, are archived from the AVN analyses and 3-hour forecasts and are provided to MOZART every three hours. MOZART is built on the framework of the transport model MATCH (Model of Atmospheric Transport and Chemistry) [*Rasch et al.*, 1997], which diagnoses convective transport [*Hack*, 1994; *Zhang and McFarlane*, 1995] and boundary layer mixing [*Holtslag and Boville*, 1993] based on the large-scale meteorological inputs. Advection of tracers is performed using the flux-form semi-Lagrangian advection scheme of *Lin and Rood* [1996] with a pressure fixer. Vertical velocities are re-diagnosed based on the continuity equation. Dry deposition velocities are calculated off-line using a resistance-in-series scheme [*Wesely*, 1989; *Hess et al.*, 2000].

[17] The chemical mechanism includes oxidation schemes for the non-methane hydrocarbons: ethane, propane, ethene, propene, isoprene, α-pinene (as a surrogate for all terpenes), and n-butane (as a surrogate for all hydrocarbons with 4 or more carbons, excluding isoprene and terpenes). Kinetic reaction rates have been updated from those used in MOZART-1 [*Brasseur et al.*, 1998], based on recent measurements, as compiled by *Sander et al.* [2000] and *Tyndall et al.* [2001]. The chemical system is solved numerically using a fully implicit Euler backward method with Newton-Raphson iteration.

[18] Surface emissions of chemical species in MOZART include those from fossil fuel burning and other industrial activity, biomass burning, biogenic emissions from vegetation and soils, and oceanic emissions, and are intended to be representative of those in the early 1990s. Emissions from fossil fuel combustion, fuelwood burning, and agricultural waste burning are based on the EDGAR v2.0 inventory [*Olivier et al.*, 1996] compiled for a base year of 1990, with seasonality from the IMAGES model [*Müller*, 1992]. For CO, emissions from agricultural waste and fuelwood burning were modified from those in EDGAR v2.0 based on preliminary estimates from EDGAR v3.0 [*Olivier and Berdowski*, 2001], by scaling to give 16 and 231 Tg/y, respectively. The spatial and temporal distribution of the amount of biomass burned is taken from *Hao and Liu* [1994] in the tropics, and from *Müller* [1992] in the extratropics. Emission ratios of chemical species from biomass burning are based on the recent review by *Andreae and Merlet* [2001]. Surface emissions of CO from fossil fuel and biomass burning sources are separately tagged based on their region of origin. We track emissions from 9 different regions: North America, South America, Europe, Africa, Australia, East Asia, South Asia, Southeast Asia, and the rest of Asia. The Asian region includes the Asian continent and Indonesia (10S–60N, 50–180E) plus the Middle East/Asia Minor. Annual CO emissions in this region are

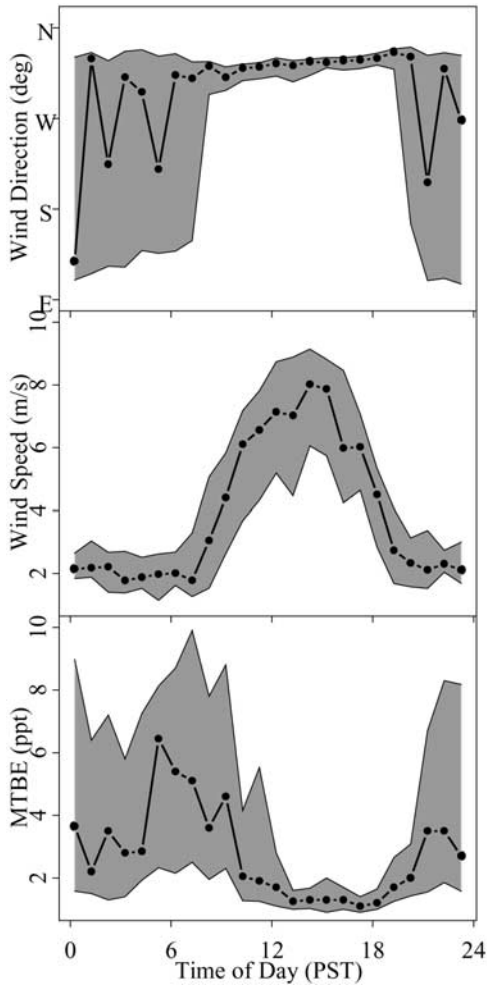


**Figure 1.** Median diurnal patterns in wind direction, wind speed and MTBE concentrations at Trinidad Head. The shaded regions bound the interquartile range [*Millet et al.*, 2004]. Time of day is presented in Pacific Standard Time (PST) in order to illustrate the typical diurnal pattern with respect to local time. Universal Time Central (UTC) is utilized in the rest of the manuscript.

99 Tg/y (fossil fuel), 147 Tg/y (biofuel) and 71 Tg/y (biomass burning). MOZART anthropogenic emissions are based on EDGAR for the early 1990s. The N. America region includes all of the United States and Canada, Central America, and the Caribbean. The European region includes all of continental Europe, Russia to 50E, and Iceland. The contribution of Asian emission sources (fossil fuel, biofuel, and biomass burning) to the MOZART $O_3$ simulation was estimated by turning off these Asian sources and subtracting the simulated ozone from the standard simulation.

[19] In this study, we sample the simulated concentrations from MOZART-2 every 3 hours from the model grid box containing Trinidad Head, taking the values from the lowest model level, which has a thickness of approximately 50 m. Total Asian emissions were summed from those originating in the areas of India, East Asia, SE Asia, and the rest of Asia.

#### 2.3.3. Backward Trajectories

[20] Three-dimensional backward trajectories were calculated with the FABtraj trajectory model using the u, v and w wind fields from the NOAA NCEP Final Analyses (FNL) [*Cooper et al.*, 2004]. The FNL data were downloaded from the National Center for Atmospheric Research data archive, available every 6-hours with a horizontal grid spacing of $1^\circ \times 1^\circ$, and 21 vertical levels between 1000 and 100 hPa. The wind field data were interpolated onto a terrain-following sigma coordinate system with horizontal grid spacing of $1^\circ \times 1^\circ$, and 22 vertical levels between the surface and 100 hPa. The three-dimensional trajectories were calculated using a linear interpolation scheme in space and time.

## 3. Results and Discussion

### 3.1. Meteorological Characteristics

[21] A regular diurnal meteorological pattern occurred during the field campaign at Trinidad Head with strong daytime winds out of the north-west (off the ocean), and weaker and more variable winds at night. As a result, air sampled during the day was typically of marine origin with little recent continental influence, whereas at night the effects of recent continental influence were commonly observed (Figure 1). The distribution of observations for wind speed and direction represented as a wind rose (Figure 2) emphasizes that winds out of the north-west were the dominant meteorological feature.

[22] The variability of all the trace gas concentrations observed at this site were closely coupled to the wind speed and direction patterns. For example, concentrations of methyl-t-butyl ether (MTBE), CO, $CO_2$, and $O_3$ are imaged as a function of both wind speed and direction in Figure 3. MTBE, CO, and $CO_2$ concentrations had similar dependencies on wind speed and direction, with enhancements for wind directions less than 140° (ENE - SE) at all wind speeds, strong enhancement around 230° (SW) at low wind speeds, and weak enhancement from 200–360° when wind speeds were low, indicating the influence of local sources. Ozone concentrations had an inverse pattern of concentration variations, suggesting that when local pollution sources were observed, ozone was depleted by surface deposition or chemical reactions. Under the dominant daytime meteorological pattern, strong winds out of the north-

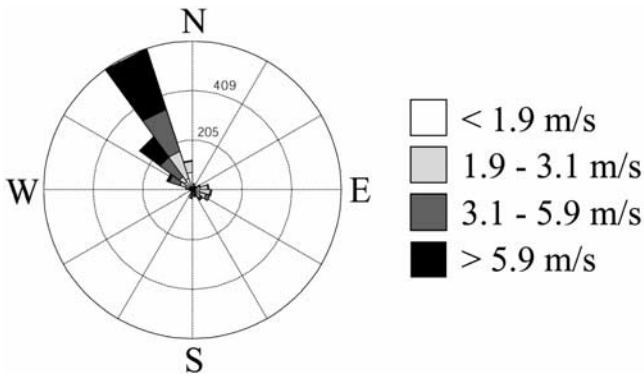


**Figure 2.** Wind rose for observations at Trinidad Head. Shading corresponds to quartiles of wind speed and the length of each bin corresponds to number of observation (scale on radial grid).

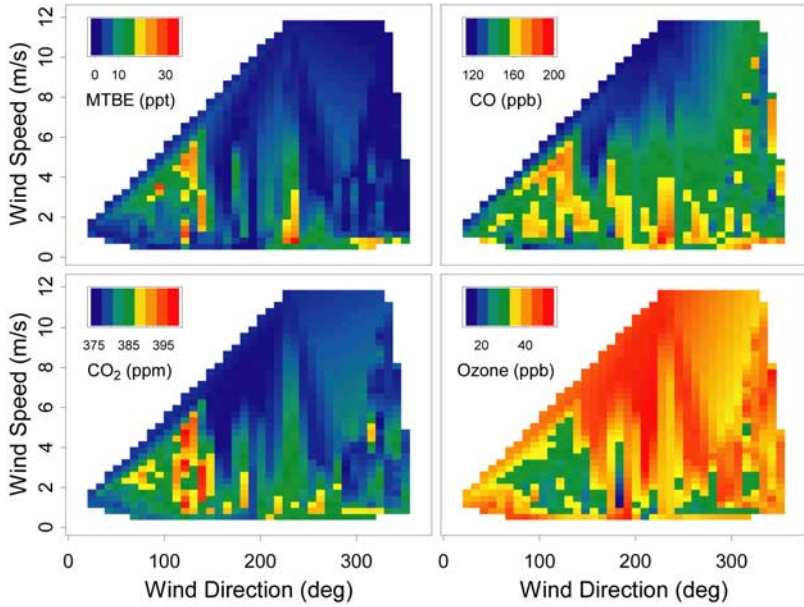


**Figure 3.** MTBE, CO, $CO_2$, and $O_3$ plotted as a function of both wind speed and direction for 20 April–22 May 2002. MTBE, CO, and $CO_2$ have high values at similar wind speeds and directions indicating the influence of local sources. Ozone concentrations show the inverse, suggesting that when local sources are observed, ozone is depleted by chemical reactions or surface deposition.

west, the concentrations of CO, $CO_2$, and MTBE were not enhanced, nor was the concentration of $O_3$ depleted.

### 3.2. Carbon Monoxide at Trinidad Head

[23] CO provides a useful tracer to evaluate the importance of intercontinental transport of pollution in springtime because it has an atmospheric lifetime (months) that is significantly longer than typical transport times across the Pacific (4–8 days), it has relatively well known source strengths, and it has been simulated with reasonable accuracy by several independent models which allow analysis of the relative importance of different sources to observed mixing ratios. Furthermore, the emission ratio relative to CO is a common metric used to estimate emissions of ozone precursors, fine particles, and other chemically and radiatively active compounds. Thus analysis of CO as a tracer for intercontinental transport of pollution provides a useful framework for considering the transport and chemistry of other species.

[24] Compounds with residence times longer than a few days whose main loss mechanism is OH chemistry have seasonally declining background concentrations in springtime at northern midlatitudes [*Goldstein et al.*, 1995; *Millet et al.*, 2004], and background CO concentrations at Trinidad Head dropped from approximately 170 ppb to 120 ppb over the 33 days of this field campaign (Figure 4b). Using observations at this site to quantify the chemical composition of air entering North America from the Pacific Ocean requires an effective method of filtering out measurements that have been impacted by recent continental emissions from North America itself, while simultaneously accounting for the seasonally declining background concentrations. In this section we explore two approaches, independent of local wind measurements, for filtering out fresh pollution sources from our analysis of long- range pollution transport. We then compare filtered CO observations to backward trajectories from the FABtraj model, and simulations from the GEOS-CHEM and MOZART models, to determine whether pollution plumes from Asia occurred and to estimate the importance of different CO emission source regions and source types to the observed mixing ratios.

### 3.3. Differentiating Fresh Versus Aged Pollution: Photochemical Clock

[25] Our first approach for differentiating between fresh regional emissions and more aged emissions was to compare observations of anthropogenically emitted hydrocarbons of varying lifetimes. For example, pentane and isopentane react faster with OH than butane, and the logarithms of the isopentane/butane and pentane/butane ratios hence decrease with time since emission, due to both photochemical oxidation and dilution with background air [*McKeen and Liu*, 1993] (Figure 4a). Fresh emissions have proportionally more of the shorter lifetime hydrocarbons, thus the upper right portion of the figure contains data that are indicative of ''Fresh'' emissions, and the lower left portion of the figure contains data that are indicative of ''Aged'' emissions. We assigned approximately one quarter of the observations as Fresh, and one quarter of the observations as Aged. Applying these Fresh and Aged photochemical criteria to the CO concentration timeline showed that nearly all of the high CO concentration observations (compared to the seasonally declining background) were associated with Fresh emissions, while much of the lower concentration CO was associated with photochemically Aged air (Figure 4b).

### 3.4. Confirmation of Backward Trajectories Using the Photochemical Clock

[26] In order to check whether backward trajectory estimates were consistent with our Fresh versus Aged

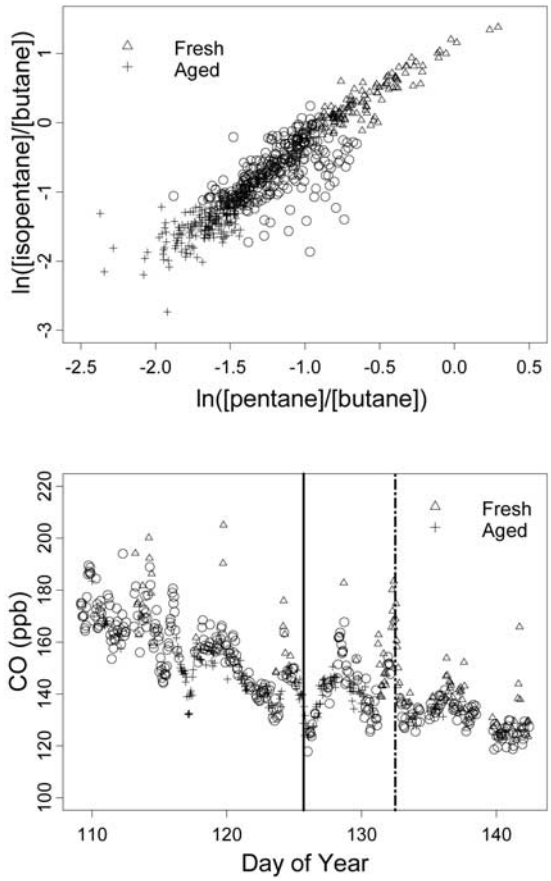


**Figure 4.** Pentane and isopentane react faster with OH than butane, therefore (a) the logarithm of pentane and isopentane to butane ratios change as a function of atmospheric oxidation and dilution, providing one measure of photochemical age of the air mass. (b) Fresh and Aged photochemical criteria applied to the CO concentration timeline show that nearly all of the high concentration CO was associated with Fresh emissions, while much of the lower concentration CO could be identified with photochemically Aged air based on the pentane to butane ratios. Solid vertical line indicates an Aged event on day 125, and dot-dashed vertical line indicates a Fresh event on day 132 for which backward trajectories are shown in Figure 5.

understanding of the history of the observed air masses, we calculated 186 hour backward trajectories initialized at Trinidad Head (950 hPa, 12:00 UTC) using the FABtraj model. Examples of these backward trajectories are shown in Figure 5 for an Aged event on day 125 (indicated by solid vertical line in Figure 4b), and a Fresh event on day 132 (indicated by dashed vertical line in Figure 4b). The backward trajectory for the Aged event on day 125 estimates that for the previous 186 hours the air mass had been in the marine boundary layer below approximately 1 km within 15° longitude of Trinidad Head before moving south-east to the measurement site. This trajectory is consistent with designation of the air mass as Aged, with strongly depleted reactive hydrocarbons and relatively low CO concentrations. The backward trajectory for the Fresh event on day 132 estimates that over the past 186 hours the air mass had descended over the western edge of North America, then stayed within 1 km of the surface as it moved southward over populated regions along the Washington and Oregon coastline before arriving at the measurement site. This trajectory is consistent with designation of the air mass as Fresh, with high levels of reactive hydrocarbons and enhanced CO concentrations. Comparison of these backward trajectory model results with the photochemical clock provides confirmation that the backward trajectories usefully estimate the history of air arriving at Trinidad Head and can provide a reasonable means to differentiate between Aged and Fresh pollution events for this measurement campaign.

### 3.5. Filtering Out Regional Influences: MTBE

[27] Our second approach for filtering out regional pollution uses observations of MTBE, a short-lived species (atmospheric lifetime ~4 days at $1 \times 10^6$ molec/cc OH) associated primarily with automotive emissions [*Schade et al.*, 2002]. MTBE levels were highest at night and in the early morning, and lowest around midday (Figure 1), and their variation with respect to wind speed and direction clearly indicated regional terrestrial anthropogenic sources (Figure 3a). Other short-lived anthropogenic compounds, such as toluene, showed similar variability with respect to diurnal patterns and wind characteristics. 2-methyl-3-buten-2-ol (MBO) is emitted by several conifer species in this region in a light and temperature dependent manner [*Schade and Goldstein*, 2001], and has no significant known anthropogenic source. MBO concentrations exhibited a pattern similar to that of the short-lived anthropogenic species such as MTBE (data not shown). The observed behavior was therefore clearly driven by the dominant wind patterns,

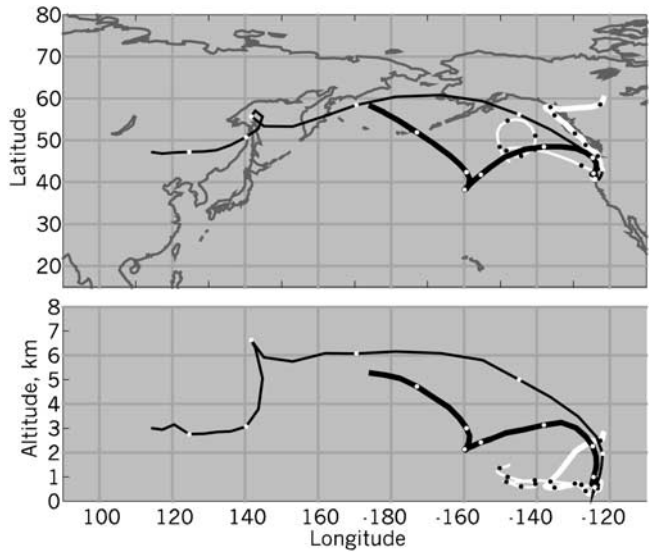


**Figure 5.** Four 186 hour backward-trajectories initialized at Trinidad Head (950 hPa, 12:00 UTC) on Day 125 (6 May, thin white line), Day 132 (12 May, thick white line), Day 118 (25 April, thin black line), and Day 136 (17 May, thick black line), 2002. Dots on the trajectories indicate each 24-hour time step.

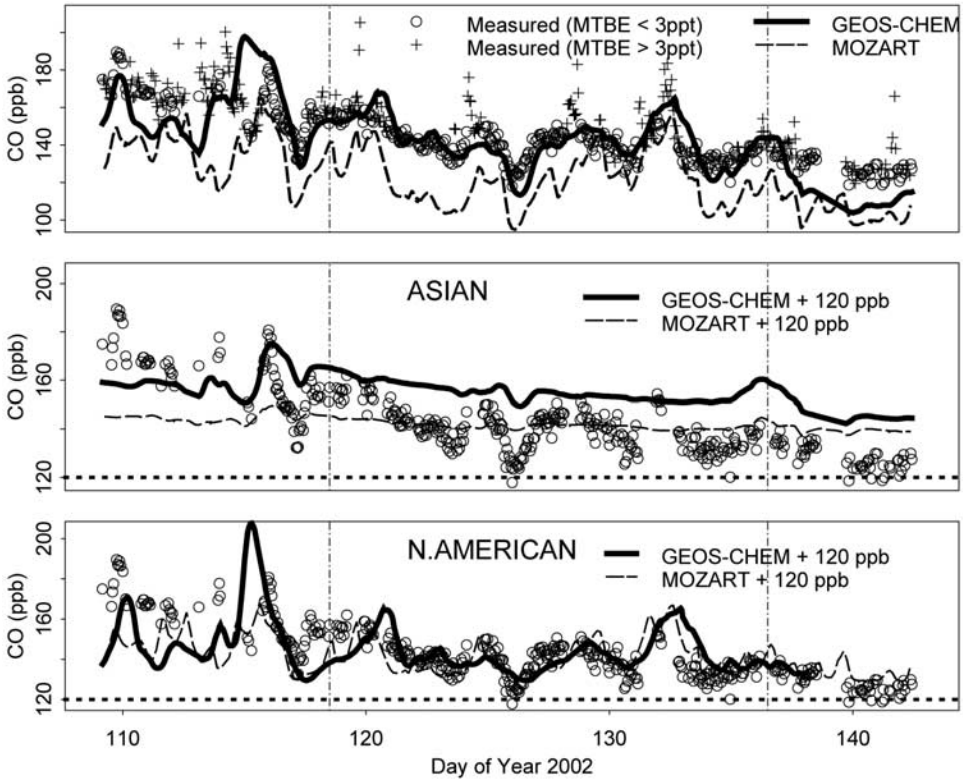


**Figure 6.** (a) CO concentration timeline differentiated by MTBE concentration indicating influence from regional emissions (filled circles, MTBE > 3 pptv) and lack of influence from regional emissions (open circles, MTBE < 3 pptv). Total CO simulated by the GEOS-CHEM and MOZART models is also shown. (b) CO timeline filtered to remove regional influences (MTBE > 3 pptv) along with GEOS-CHEM and MOZART model simulations of CO from Asia. (c) CO timeline filtered to remove regional influences (MTBE < 3 pptv) along with GEOS-CHEM and MOZART model simulations of CO from North America. In panels (b) and (c) 120 ppb CO was added to the model simulations to allow comparison of predicted and observed variability. The variability of observed CO agrees well with both model simulations for North American contributions. Vertical lines at day 118.5 and 136.5 indicate the most likely times when the influence of Asian emissions may have been discernable as plumes, and backward trajectories are shown for these times in Figure 5.

whereby recent continental influence, whether anthropogenic or biogenic, was observed with offshore flow or under stagnant conditions.

[28] Following *Millet et al.* [2004] we assigned 3 ppt MTBE as a threshold to separate between minimal local influence (60% of observations) and recently polluted air (40% of observations) to filter out significant influences from North American continental emissions. Although 40% of the data were excluded by this analysis, the resulting mean CO concentration decreased by only 5 ppb, or 3.4% (147 ± 16 ppb unfiltered, 142 ± 14 ppb filtered, mean ± standard deviation). Periods with MTBE < 3 ppt were dominantly associated with flow from the northwest, however, the MTBE filter also excluded some data associated with onshore winds, and included some data with offshore winds. Chemical tracers such as MTBE are more effective for filtering out local influences than local wind measurements or backward trajectory analysis. Instantaneous wind-measurements do not necessarily provide an accurate indicator of air mass history, and backward trajectory analysis is typically less certain near the surface than aloft and also cannot provide as high time resolution as is possible using measured VOC tracers. The removal of regional influences on CO observations utilizing the 3 ppt MTBE filter is illustrated in Figure 6a.

### 3.6. Observed CO Compared to Model Simulations

[29] Observed CO concentrations, filtered to indicate regional emissions (MTBE > 3ppt), are compared to GEOS-CHEM and MOZART model simulations for total CO in Figure 6a. The GEOS-CHEM model simulated both the temporal variability and the absolute magnitude of total CO concentrations extremely accurately. The MOZART model simulated nearly identical temporal variability, but the absolute magnitude of CO was lower than the filtered observations by 19 ppb on average.

[30] Both models can tag CO from different emission regions and source types. These models therefore provide an opportunity to estimate the contributions to CO from all the major source regions and source types, and to explore why the simulations differ. Comparisons of model simulations for contributions from Asian and North American emissions are shown in Figures 6b and 6c, respectively. The GEOS-CHEM and MOZART models simulated significantly different mean contributions from Asia of 48 ± 7

**Table 1.** Contributions to Mean Observed CO

| Observations | Mixing Ratios | |
|---|---|---|
| Mean Observed CO | 147 ppb | |
| Mean Filtered CO (MTBE < 3 ppt) | 142 ppb[a] | |
| Model Simulations | GEOS-CHEM | MOZART |
| Asian Fossil Fuel + Biofuel[b] | 35 ppb (25%)[c] | 12 ppb (8%) |
| Asian Biomass Burning + Biofuel | 13 ppb (9%) | 10 ppb (7%) |
| N. Amer. Fossil Fuel + Biomass Burning | 26 ppb (19%) | 21 ppb (15%) |
| European Fossil Fuel + Biomass Burning | 19 ppb (13%) | 13 ppb (9%) |
| Photochemical + natural + other anthrop. | 46 ppb (32%) | 67 ppb (47%) |
| Total | 139 ppb (98%) | 123 ppb (87%) |

[a]MTBE > 3 ppt indicates contributions from local CO sources that the models do not simulate.
[b]GEOS-CHEM includes biofuel emission with fossil fuel emission, MOZART includes biofuel emission with biomass burning emission.
[c]Percentage of observed CO (mean filtered) follows ppb contributions.

and 22 ± 2 ppb (mean ± standard deviation) respectively. It is clear that the difference in Asian fossil fuel emissions is the main difference between the total CO simulations (Table 1).

[31] Emissions of CO used in the GEOS-CHEM simulation included: Global fossil fuel (395 Tg/yr), biofuel (160 Tg/yr), and biomass burning (420 Tg/yr), and Asian fossil fuel (165 Tg/yr), biofuel (90 Tg/yr), and biomass burning (120 Tg/yr). Emissions used in the MOZART simulation included: Global fossil fuel (307 Tg/y), biofuel (231 Tg/y), biomass burning (480 Tg/y), and Asian fossil fuel (99 Tg/y), and biofuel plus biomass burning (219 Tg/y). Analyses of observations from the TRACE-P campaigns showed that the *Streets et al.* [2003] inventory for anthropogenic Chinese emissions is too low, by approximately 50% [*Carmichael et al.*, 2003; *Palmer et al.*, 2003]. The CO emissions used in GEOS-CHEM [from *Duncan et al.*, 2003] are about 50% higher than *Streets et al.* [2003] in China and give an unbiased simulation of Asian outflow observations in TRACE-P [*Li et al.*, 2004; *Heald et al.*, 2003]. It appears that Asian fossil fuel emissions used in the MOZART model are also lower than necessary to match the observations at Trinidad Head, and are probably comparable to those used by *Streets et al.* [2003].

[32] The two models simulate similar temporal variability in the Asian CO component (Figure 6b). Although there are some similar features in observed total CO and modeled Asian CO, modeled Asian emissions did not account for the observed CO variability at Trinidad Head. The simulated mean contribution of North American CO (26 ± 13 ppb for GEOS-CHEM and 21 ± 9 ppb for MOZART), mostly due to fossil fuel consumption, is lower than the simulated contribution from Asia, yet the variability is much higher and the North American contribution simulated by both models closely matches the observed temporal variability in filtered CO (Figure 6c). From this comparison, we infer that the total contribution from Asian emissions to observed CO was significantly larger than the contribution from North America, but that the Asian contribution was relatively constant while the North American contribution caused most of the temporal variability in the observed concentrations.

[33] Much of the recent published research addressing impacts of Asian emissions on air quality in North America has focused on events (typically in springtime) when pollution plumes originating in Asia have been observed over the western Pacific Ocean or the west coast of North America [e.g., *Jaffe et al.*, 2003a]. On the basis of our comparison of the GEOS-CHEM and MOZART models with observations during spring 2002 at Trinidad Head, we conclude that Asian pollution events may be hard to distinguish at North American ground sites, but that Asian emissions nonetheless provide the dominant direct emission contribution to observed CO, accounting for approximately one third of the total mixing ratios.

[34] We further examined the CO observations to determine whether any specific Asian plume events occurred. The three days with highest model-predicted contribution from Asia were 116, 118, and 136. Day 116 was also toward the end of a period when the model predicted the highest contribution from North America, thus it was impossible to infer from the modeled versus measured concentrations where this high CO originated. We identified the remaining two days as the most likely times when influence from Asian emissions may have been discernable as plumes, as the model-predicted variability in Asian CO was larger than the variability in North American CO and North American CO contributions were predicted to be small. Chosen times are indicated by vertical lines at day 118.5 and 136.5 in Figure 6, and 186 hour backward-trajectories for these times initialized at Trinidad Head (950 hPa) using the FABtraj model are shown in Figure 5. The backward trajectory for day 118 shows that air rose over Asia, was transported quickly across the pacific, then descended north of Trinidad Head and traveled slightly inland before reaching Trinidad Head. The CO concentration at this time was not obviously elevated above the ''background'' concentration (Figure 6a) and the MTBE filter indicated local emissions had impacted the air mass, even though the GEOS-CHEM and MOZART models predicted that contributions from North America would be minimal at this time. The contribution from Asian emissions to total observed CO at this time may have been large, but it did not cause a clear enhancement over ''background'' CO concentrations. The 186 hour backward trajectory for day 136 originated over the North Pacific, moved southwest, then west, and descended to the surface north of Trinidad Head before arriving at the measurement site. The MTBE filter again indicated that local emissions were added to this air mass before it reached Trinidad Head, and the CO concentrations were again not clearly elevated over the ''background'' concentrations (Figure 6a). We conclude that no clearly discernable CO plumes from Asia arrived at Trinidad Head during this field campaign.

[35] It is likely that pollution plumes from Asia were transported at higher altitude but did not reach the ground at Trinidad Head during this field campaign. Evidence for these plumes has been repeatedly observed. For example, *Jaffe et al.* [2003a] summarize observations in the free troposphere over the U.S. west coast with evidence of coherent plumes of Asian pollution, most prominently CO. *Yienger et al.* [2000], using a global chemistry transport model, estimated that major Asian pollution events are very common in the mid- and upper troposphere above the U.S., but perhaps only 3–5 of these events directly impact the

atmospheric boundary layer along the U.S. west coast during a typical February–May period. This transport is discussed in detail for the ITCT campaign by *Forster et al.* [2004] and *Cooper et al.* [2004].

[36] Although the variability of CO concentrations observed at Trinidad Head was dominated by North American sources and regional emissions not captured by the models, and the major impact of Asian emissions could not be observed in pollution events at the surface, the match between the simulationed and observed CO concentrations still suggests that we can use the models to differentiate the mean contributions to total observed CO. Simultaneous observations made at Cheeka Peak on the coast of Washington state also showed good agreement with GEOS-CHEM simulations, bolstering this argument. In addition, at Cheeka Peak the model not only predicted the seasonal variability of background CO, it also captured observed enhancements during long-range transport events from Asia [*Jaeglé et al.*, 2003].

[37] The impact of Asian emissions should be evaluated in terms of their impact on total observed concentrations. The mean observed CO at Trinidad Head was 147 ppb, with only 5 ppb (3%) coming from local emissions as determined using the MTBE filter. The MOZART and GEOS-CHEM models simulated that the dominant northern hemisphere direct emission contributions to the observed CO were from Asia (15 and 33% respectively, with 33% being more likely given the better agreement between GEOS-CHEM simulated and observed total CO), North America (15 and 19%), and Europe (9 and 13%), with the remainder coming from photochemical production, natural sources, and anthropogenic emissions from other regions (47 and 32% simulated by both models) (Table 1).

### 3.7. Ozone at Trinidad Head

[38] A major reason for concern over rising emissions due to industrialization in Asia is the potential impact on ozone and ozone precursor concentrations in air entering western North America from the Pacific. *Jacob et al.* [1999] predicted that the expected tripling of Asian emissions from 1985–2010 would result in an increase in monthly mean surface ozone of 2–6 ppb in the western U.S. However, *Jaffe et al.* [2003b] showed evidence suggesting that ozone levels in air entering western North America had increased approximately 10 ppb between 1984 and 2002, substantially more than the total $O_3$ due to Asian emissions predicted by *Jacob et al.* [1999]. Therefore it is important to understand the processes controlling ozone concentrations observed at sites on the west coast of North America in order to discern potential influences from long- range transport of ozone and ozone precursors.

[39] The variability in $O_3$ concentrations observed at Trinidad Head was negatively correlated with many directly emitted biogenic and anthropogenic trace gases (e.g., Figure 3). The highest $O_3$ concentrations were coincident with the lowest concentrations of $CO_2$ (Figures 3 and 7). This behavior is consistent with $CO_2$ from local or regional respiration sources building up near the ground when the boundary layer was shallow and mixing was very limited (mainly at night with weak offshore flow) and ozone concentrations simultaneously decreasing due to surface deposition or possibly gas phase chemical losses. A similar

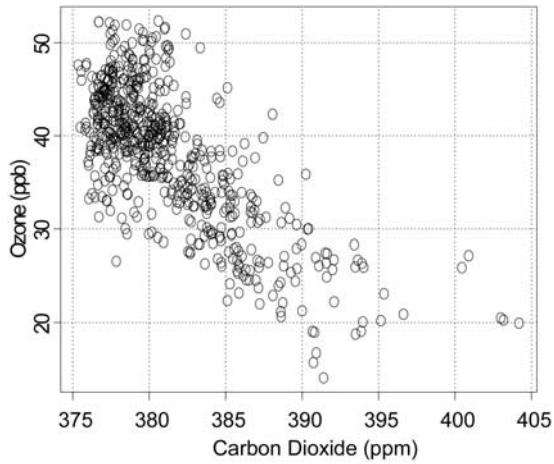


**Figure 7.** Negative correlation of $CO_2$ with $O_3$ for the whole field measurement campaign. Ozone concentration mainly varied with stability and wind direction as indicated by the buildup of respired (or regionally emitted) $CO_2$.

negative correlation was observed for $O_3$ versus radon (data not shown), suggesting that the ozone decreases in the shallow mixed layer were due to processes involving the local terrestrial ecosystems rather than the ocean surface. During periods of enhanced vertical mixing and/or onshore flow, the impact of loss processes within the boundary layer on surface $O_3$ concentrations decreased, which in conjunction with photochemical production typically increased $O_3$ levels to a late afternoon maximum.

[40] The timeline of ozone concentrations is shown in Figure 8 with solid vertical lines indicating one high ozone period (Day 117) and one low ozone period (Day 113), for which vertical profiles from ozone sondes are shown in Figure 9. Periods with low ozone levels corresponded to stable situations with a shallow mixed layer, which led to ozone loss near the ground. It is clear that mixing processes controlled the observed variability of surface $O_3$ concentrations at Trinidad Head, and that ground-based measurements were only indicative of concentrations at higher altitudes during well mixed time periods. This decoupling between the marine boundary layer and the transport and chemistry of air at higher altitudes is probably typical of the west coast of North America. This idea is supported by consistent and frequent observations of aerosols from Asia in ground-based samples collected at montane sites at altitudes which are typically above the marine boundary layer in western North America, and lack of similar Asian aerosols in samples collected at sites in coastal areas below this altitude [*VanCuren and Cahill*, 2002; *VanCuren*, 2003].

[41] The strong anti-correlation between $CO_2$ and $O_3$ provided a useful method to filter out local influences on observed $O_3$ concentrations. We filtered our observations to remove local depletions in $O_3$ ($CO_2 > 383$ ppm) in order to compare observations with GEOS-CHEM and MOZART model predictions only during well mixed time periods when the model resolution would be more appropriate for predicting surface $O_3$ concentrations (Figure 8). The mean and the statistical variability of total $O_3$ simulated by the GEOS-CHEM model (39 ± 5 ppb, mean ± standard deviation) and the MOZART model (37 ± 9 ppb) were in

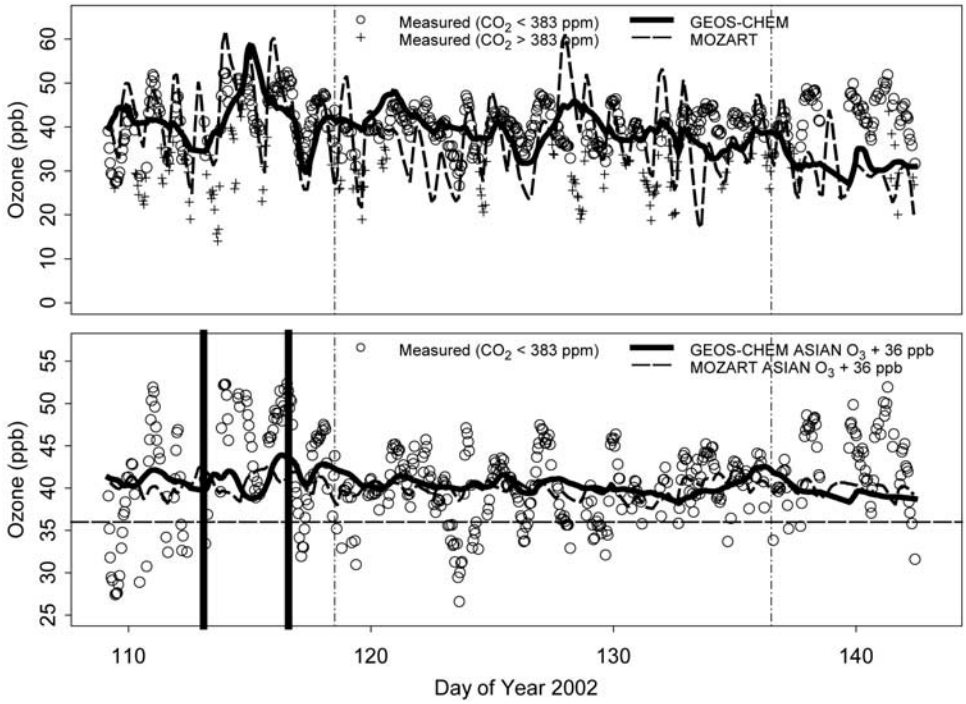


**Figure 8.** (a) Ozone concentration timeline differentiated by $CO_2$ concentration indicating times when vertical stability caused local decreases in $O_3$ (pluses, $CO_2$ > 383 ppm), and times with stronger vertical mixing (open circles, $CO_2$ < 383 ppm). Total $O_3$ simulated by the GEOS-CHEM and MOZART models are also shown. (b) $O_3$ timeline filtered to remove regional influences ($CO_2$ > 383 ppm) along with GEOS-CHEM and MOZART model simulations of $O_3$ produced from Asian emissions. 36 ppb $O_3$ was added to the model simulation to allow comparison of predicted and observed variability. Solid vertical lines indicate one high ozone period (Day 117) and one low ozone period (Day 113) for which vertical profiles from ozone sondes are shown in Figure 9. Dot-dashed vertical lines at days 118.5 and 136.5 indicate the most likely times that the influence of Asian emissions may have been discernable as plumes, and backward trajectories are shown for these times in Figure 5.

reasonable agreement with both the filtered $O_3$ observations (41 ± 5 ppb) and the unfiltered $O_3$ observations (38 ± 7 ppb) (Figure 8). However, neither model did a very good job of matching the observed temporal variability in $O_3$.

[42] Model simulated $O_3$ due to emissions of $O_3$ precursors from Asia (Figure 8b) was relatively constant for both GEOS-CHEM (4.5 ± 1.1 ppb, mean ± standard deviation) and MOZART (4.2 ± 1.3 ppb) compared to the observed variability in $O_3$. The mean simulated contribution from Asia for both models was 10–11% of the observed $O_3$ concentrations. This simulated contribution was significantly smaller than the approximately 10 ppb increase reported by *Jaffe et al.* [2003b] during springtime between 1984 and 2002, suggesting disagreement between observed trends in $O_3$ that have been attributed to rising Asian emissions and model-predicted current $O_3$ contributions from Asia calculated for the ITCT time period. This discrepancy between observations of $O_3$ and attribution of those observations to specific causes, and ozone source partitioning by current models, is worthy of further investigation.

[43] We further examined the $O_3$ observations to determine whether any specific Asian plume events could be identified using backward-trajectories. The vertical lines at day 118.5 and 136.5 in Figure 8 indicate the times defined above as the most likely periods of discernable ground level pollution enhancement due to trans-Pacific transport of a

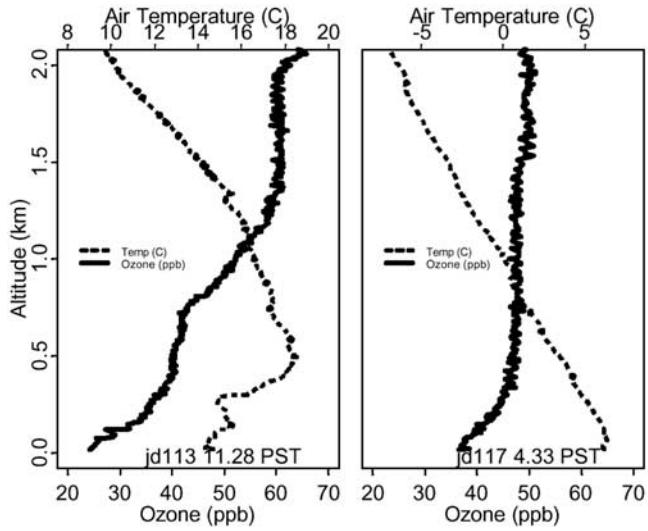


**Figure 9.** Ozone concentration and air temperature as a function of altitude measured by balloon borne ozone sondes for one low ozone period (Day 113, left panel) and one high ozone period (Day 117, right panel). These ozone sondes confirm that ozone concentrations at the ground were highly dependent on vertical stability with maximum concentrations observed during times of strongest vertical mixing, and lowest concentrations observed when vertical mixing was suppressed.

coherent Asian plume. The $O_3$ concentrations observed at these times showed no elevations above the "background" concentration. At no time during the measurement campaign was there a combination of elevated ozone concentrations and a backward-trajectory indicative of transport from Asia.

## 4. Conclusions

[44] Measurements for a wide suite of trace gases and aerosols were made at Trinidad Head, California, from 19 April through 22 May 2002 as part of the NOAA ITCT research program. We used these data to elucidate the influence of Asian emissions on air masses entering North America in springtime. CO has been identified as one of the most useful tracers to look for Asian emission plumes because of its relatively long atmospheric lifetime and its emission from all combustion sources. $O_3$ is a secondary air pollutant whose concentration is regulated, and thus potential enhancement of North American $O_3$ due to Asian emissions is a serious concern for air quality control. Before assessing the influence of long- range transport on the observed mixing ratios for these gases, the efficacy of backward-trajectories for discerning the history of air masses arriving at the site was addressed, and local/regional influences impacting observations at Trinidad Head were filtered out of the data set. A hydrocarbon photochemical clock proved to be a useful means for differentiating between Fresh and Aged pollution, and was used to confirm that calculated backward trajectories indeed represented the history of air masses arriving at Trinidad Head. MTBE was shown to be a useful filter for local/regional influences due to its association with fossil fuel use and its atmospheric lifetime of a few days. $CO_2$ also was shown to be a useful tracer of regional continental influences when concentrations were enhanced due to emissions under stable atmospheric conditions. Filtering out local influences removed 20 to 40% of the observations, depending on the constraints applied, decreased the mean CO mixing ratio by 5%, and increased the mean $O_3$ mixing ratio by 8%.

[45] After filtering the data to remove local influences, the variability and the absolute concentration in the remaining data was examined for Asian influence by comparison with GEOS-CHEM and MOZART model simulations run as part of the ITCT campaign. The observed variability in the filtered CO data was well simulated using the GEOS-CHEM model in terms of both temporal variability and absolute concentration. The CO simulation using MOZART also captured the temporal variability in the filtered observations, but the absolute concentration was approximately 19 ppb too low. The main difference in model simulated CO was in the fossil fuel contribution from Asia, with MOZART simulating 23 ppb lower CO than GEOS-CHEM (12 versus 35 ppb). We infer that the emission inventory used for this term in the MOZART model was too low, and correcting it would largely account for the discrepancy from the observed CO. The two models agreed that North American fossil fuel emissions explained the vast majority of the variability in CO concentrations observed at Trinidad Head. Distinct Asian pollution plumes did not impact these ground-based observations, because the magnitude of CO variability due to Asian emissions was small relative to the total observed variability.

[46] Although the variability of CO concentrations observed at Trinidad Head was dominated by North American sources, and the Asian emissions did not cause observable plumes, the match between the GEOS-CHEM and MOZART simulations and observed CO concentrations provide confidence that it is reasonable to use the models to differentiate the mean contributions to total observed CO. The MOZART and GEOS-CHEM models agreed that the dominant northern hemisphere direct emission contributions to the observed CO were from Asia (15 and 33% respectively, with 33% being more likely given the better agreement between GEOS-CHEM simulated and observed total CO), North America (15 and 19%), and Europe (9 and 13%), with the remainder coming from photochemical production, natural sources, and anthropogenic emissions from other regions (47 and 32%). We conclude that Asia provided the dominant source of direct emissions contributing to the observed CO at Trinidad Head during springtime, accounting for approximately one third of the total.

[47] Ozone concentrations varied with local atmospheric stability as indicated by tracers such as $CO_2$ and vertical profiles measured by ozone sondes, and were not impacted by Asian plumes. On the basis of both the GEOS-CHEM and MOZART model simulation we conclude that on average 10% ($4 \pm 1$ ppb) of $O_3$ observed at Trinidad Head was produced from ozone precursors emitted in Asia.

[48] Because Asian plumes have only been identified for approximately 20 episodes over more than a decade, and similar plumes were not observed during our field campaign at Trinidad Head, we conclude that the contributions of Asian emissions to the persistent background is a much more important issue than the frequency of plumes, with more significant implications for air quality control in North America.

[49] **Acknowledgments.** This work was supported by the NOAA Office of Global Programs (grant NA16GP2314). Dylan Millet thanks the DOE Global Change Education program for a GREF fellowship. The authors thank David Parrish and two anonymous reviewers for helpful feedback on the manuscript.

## References

Allan, J. D., J. L. Jimenez, P. I. Williams, M. R. Alfarra, K. N. Bower, J. T. Jayne, H. Coe, and D. R. Worsnop (2003), Quantitative sampling using an Aerodyne aerosol mass spectrometer: 1. Techniques of data interpretation and error analysis, *J. Geophys. Res.*, *108*(D3), 4090, doi:10.1029/2002JD002358.

Andreae, M. O., and P. Merlet (2001), Emission of trace gases and aerosols from biomass burning, *Global Biogeochem. Cycles*, *15*(4), 955–966.

Andreae, M. O., H. Berresheim, T. W. Andreae, M. A. Kritz, T. S. Bates, and J. T. Merrill (1988), Vertical distribution of dimethylsulfide, sulfur dioxide, aerosol ions, and radon over the northeast Pacific Ocean, *J. Atmos. Chem.*, *6*(1–2), 149–173.

Bench, G., P. G. Grant, D. Ueda, S. S. Cliff, K. D. Perry, and T. A. Cahill (2002), The use of STIM and PESA to respectively measure profiles of aerosol mass and hydrogen content across mylar rotating drug impactor samples, *Aerosol Sci. Technol.*, *36*, 642–651.

Berntsen, T. K., S. Karlsdottir, and D. A. Jaffe (1999), Influence of Asian emissions on the composition of air reaching the North Western United States, *Geophys. Res. Lett.*, *26*(14), 2171–2174.

Bey, I., D. J. Jacob, R. M. Yantosca, J. A. Logan, B. D. Field, A. M. Fiore, Q. Li, H. Y. Liu, L. J. Mickley, and M. G. Schultz (2001a), Global modeling of tropospheric chemistry with assimilated meteorology: Model description and evaluation, *J. Geophys. Res.*, *106*(D19), 23,073–23,096.

Bey, I., D. J. Jacob, J. A. Logan, and R. M. Yantosca (2001b), Asian chemical outflow to the Pacific: Origins, pathways and budgets, *J. Geophys. Res.*, *106*(D21), 23,097–23,114.

Brasseur, G. P., D. A. Hauglustaine, S. Walters, P. J. Rasch, J. F. Muller, C. Granier, and X. X. Tie (1998), MOZART, a global chemical transport model for ozone and related chemical tracers: 1. Model description, *J. Geophys. Res.*, *103*, 28,265–28,289.

Cahill, T. A., and P. Wakabayashi (1993), Compositional analysis of size-segregated aerosol samples, in *Measurement Challenges in Atmospheric Chemistry*, *Am. Chem. Soc. Adv. in Chem. Ser.*, vol. 232, edited by L. Newman, pp. 211–228, Oxford Univ. Press, New York.

Carmichael, G. R., et al. (2003), Evaluating regional emission estimates using the TRACE-P observations, *J. Geophys. Res.*, *108*(D21), 8810, doi:10.1029/2002JD003116.

Cooper, O. R., et al. (2004), A case study of transpacific warm conveyor belt transport: Influence of merging airstreams on trace gas import to North America, *J. Geophys. Res.*, *109*, D23S08, doi:10.1029/2003JD003624, in press.

Duncan, B. N., R. V. Martin, A. C. Staudt, R. M. Yevich, and J. A. Logan (2003), Interannual and seasonal variability of biomass burning emissions constrained by satellite observations, *J. Geophys. Res.*, *108*(D2), 4100, doi:10.1029/2002JD002378.

Forster, C., et al. (2004), Lagrangian transport model forecasts and a transport climatology for the Intercontinental Transport and Chemical Transformation 2002 (ITCT 2K2) measurement campaign, *J. Geophys. Res.*, *109*, D07S92, doi:10.1029/2003JD003589.

Goldstein, A. H., S. C. Wofsy, and C. M. Spivakovsky (1995), Seasonal variations of nonmethane hydrocarbons in rural New England: Constraints on OH concentrations in northern midlatitudes, *J. Geophys. Res.*, *100*(D10), 21,023–21,033.

Hack, J. J. (1994), Parametrization of moist convection in the National Center for Atmospheric Research community climate model (CCM2), *J. Geophys. Res.*, *99*(D3), 5541–5568.

Hao, W. M., and M. H. Liu (1994), Spatial and temporal distribution of tropical biomass burning, *Global Biogeochem. Cycles*, *8*(4), 495–503.

Heald, C. L., et al. (2003), Asian outflow and trans-Pacific transport of carbon monoxide and ozone pollution: An integrated satellite, aircraft, and model perspective, *J. Geophys. Res.*, *108*(D24), 4804, doi:10.1029/2003JD003507.

Hess, P. G., S. Flocke, J. F. Lamarque, M. C. Barth, and S. Madronich (2000), Episodic modeling of the chemical structure of the troposphere as revealed during the spring MLOPEX 2 intensive, *J. Geophys. Res.*, *105*(D22), 26,809–26,839.

Hoell, J. M., D. D. Davis, S. C. Liu, R. E. Newell, H. Akimoto, R. J. McNeal, and R. J. Bendura (1997), The Pacific Exploratory Mission West phase B: February–March, 1994, *J. Geophys. Res.*, *102*(D23), 28,223–28,239.

Holtslag, A. A. M., and B. A. Boville (1993), Local versus nonlocal boundary layer diffusion in a global climate model, *J. Clim.*, *6*(10), 1825–1842.

Horowitz, L. W., et al. (2003), A global simulation of tropospheric ozone and related tracers: Description and evaluation of MOZART, version 2, *J. Geophys. Res.*, *108*(D24), 4784, doi:10.1029/2002JD002853.

Husar, R. B., et al. (1998), Asian dust events of April 1998, *J. Geophys. Res*, *106*(D16), 18,317–18,330.

Jacob, D. J., J. A. Logan, and P. P. Murti (1999), Effect of rising Asian emissions on surface ozone in the United States, *Geophys. Res. Lett.*, *26*(14), 2175–2178.

Jaeglé, L., D. A. Jaffe, H. U. Price, P. Weiss-Penzias, P. I. Palmer, M. J. Evans, D. J. Jacob, and I. Bey (2003), Sources and budgets for CO and $O_3$ in the northeastern Pacific: Results from the PHOBEA-II Experiment, *J. Geophys. Res.*, *108*(D20), 8802, doi:10.1029/2002JD003121.

Jaffe, D., et al. (1999), Transport of Asian air pollution to North America, *Geophys. Res. Lett.*, *26*(6), 711–714.

Jaffe, D., I. McKendry, T. Anderson, and H. Price (2003a), Six 'new' episodes of trans-Pacific transport of air pollutants, *Atmos. Environ.*, *37*(3), 391–404.

Jaffe, D., H. Price, D. Parrish, A. Goldstein, and J. Harris (2003b), Increasing background ozone during spring on the west coast of North America, *Geophys. Res. Lett.*, *30*(12), 1613, doi:10.1029/2003GL017024.

Jimenez, J. L., et al. (2003), Ambient aerosol sampling using the Aerodyne Aerosol Mass Spectrometer, *J. Geophys. Res.*, *108*(D7), 8425, doi:10.1029/2001JD001213.

Kritz, M., J. C. Leroulley, E. Danielsen, and G. Lambert (1988), The China Clipper: Fast advective transport of radon-rich air from the Asian boundary layer to the upper troposphere near California, *Chem. Geol.*, *70*(1–2), 96.

Li, Q., et al. (2002), Transatlantic transport of pollution and its effects on surface ozone in Europe and North America, *J. Geophys. Res.*, *107*(D13), 4166, doi:10.1029/2001JD001422.

Li, Q. B., D. J. Jacob, R. M. Yantosca, J. W. Munger, and D. D. Parrish (2004), Export of $NO_y$ from the North American boundary layer: Reconciling aircraft observations and global model budgets, *J. Geophys. Res.*, *109*, D02313, doi:10.1029/2003JD004086.

Lin, S. J., and R. B. Rood (1996), Multidimensional flux-form semi-Lagrangian transport schemes, *Mon. Weather Rev.*, *124*(9), 2046–2070.

Liu, H., D. J. Jacob, L. Y. Chan, S. J. Oltmans, I. Bey, R. M. Yantosca, J. M. Harris, B. N. Duncan, and R. V. Martin (2002), Sources of tropospheric ozone along the Asian Pacific Rim: An analysis of ozonesonde observations, *J. Geophys. Res.*, *107*(D21), 4573, doi:10.1029/2001JD002005.

Liu, H., D. J. Jacob, I. Bey, R. M. Yantosca, B. N. Duncan, and G. W. Sachse (2003), Transport pathways for Asian pollution outflow over the Pacific: Interannual and seasonal variations, *J. Geophys. Res.*, *108*(D20), 8786, doi:10.1029/2002JD003102.

McKeen, S. A., and S. C. Liu (1993), Hydrocarbon ratios and photochemical history of air masses, *Geophys. Res. Lett.*, *20*(21), 2363–2366.

McKendry, I. G., J. P. Hacker, R. Stull, S. Sakiyama, D. Mignacca, and K. Reid (2001), Long-range transport of Asian dust to the Lower Fraser Valley, British Columbia, Canada, *J. Geophys. Res.*, *106*(D16), 18,361–18,370.

Millet, D. B., et al. (2004), Volatile organic compound measurements at Trinidad Head, California, during ITCT 2K2: Analysis of sources, atmospheric composition, and aerosol residence times, *J. Geophys. Res.*, *109*, D23S16, doi:10.1029/2003JD004026, in press.

Müller, J. F. (1992), Geographical distribution and seasonal variation of surface emissions and deposition velocities of atmospheric trace gases, *J. Geophys. Res.*, *97*(D4), 3787–3804.

Olivier, J. G. J., and J. J. M. Berdowski (2001), Global emission sources and sinks, in *The Climate System*, edited by J. Berdowski, R. Guicherit, and B. J. Heij, pp. 33–77, Swets and Zeitlinger, Lisse, Netherlands.

Olivier, J. G. J., A. F. Bouwman, C. W. M. v. d. Maas, J. J. M. Berdowski, C. Veldt, J. P. J. Bloos, A. J. H. Visschedijk, P. Y. J. Zandveld, and J. L. Haverlag (1996), Description of EDGAR version 2. 0: A set of global emission inventories of greenhouse gases and ozone-depleting substances for all anthropogenic and most natural sources on a per country basis and on a 1 × 1 degree grid, *RIVM report 771060002/TNO, rep. R96/119*, Natl. Inst. of Public Health and the Environ., Bilthoven, Netherlands.

Orsini, D. A., Y. L. Ma, A. Sullivan, B. Sierau, K. Baumann, and R. J. Weber (2003), Refinements to the particle-into-liquid sampler (PILS) for ground and airborne measurements of water soluble aerosol composition, *Atmos. Environ.*, *37*(9–10), 1243–1259.

Palmer, P. I., D. J. Jacob, D. B. A. Jones, C. L. Heald, R. M. Yantosca, J. A. Logan, G. W. Sachse, and D. G. Streets (2003), Inverting for emissions of carbon monoxide from Asia using aircraft observations over the western Pacific, *J. Geophys. Res.*, *108*(D21), 8828, doi:10.1029/2003JD003397.

Parrish, D. D., C. J. Hahn, E. J. Williams, R. B. Norton, F. C. Fehsenfeld, H. B. Singh, J. D. Shetter, B. W. Gandrud, and B. A. Ridley (1992), Indications of photochemical histories of Pacific air masses from measurements of atmospheric trace species at Point Arena, California, *J. Geophys. Res.*, *97*(D14), 15,883–15,901.

Parrish, D. D., J. S. Holloway, M. Trainer, P. C. Murphy, G. L. Forbes, and F. C. Fehsenfeld (1993), Export of North American ozone pollution to the north Atlantic Ocean, *Science*, *259*(5100), 1436–1439.

Penkett, S. A., A. Volz-Thomas, D. D. Parrish, R. E. Honrath, and F. C. Fehsenfeld (1998), Special section: North Atlantic Regional Experiment (NARE II): Preface, *J. Geophys. Res.*, *103*(D11), 13,353–13,355.

Perry, K. D., T. A. Cahill, R. C. Schnell, and J. M. Harris (1999), Long-range transport of anthropogenic aerosols to the national Oceanic and Atmospheric Administration baseline station at Mauna Loa Observatory, Hawaii, *J. Geophys. Res.*, *104*(D15), 18,521–18,533.

Rasch, P. J., N. M. Mahowald, and B. E. Eaton (1997), Representations of transport, convection, and the hydrologic cycle in chemical transport models: Implications for the modeling of short-lived and soluble species, *J. Geophys. Res.*, *102*(D23), 28,127–28,138.

Sander, S. P., et al. (2000), *Chemical Kinetics and Photochemical Data for Use in Stratospheric Modeling, Supplement to Evaluation 12: Update of Key Reactions*, Jet Propulsion Lab., Pasadena, Calif.

Schade, G. W., and A. H. Goldstein (2001), Fluxes of oxygenated volatile organic compounds from a ponderosa pine plantation, *J. Geophys. Res.*, *106*(D3), 3111–3123.

Schade, G. W., G. B. Dreyfus, and A. H. Goldstein (2002), Atmospheric methyl-tertiary-butyl- ether (MTBE) at a rural mountain site in California, *J. Environ. Qual.*, *31*, 1088–1094.

Streets, D. G., et al. (2003), An inventory of gaseous and primary aerosol emissions in Asia in the year 2000, *J. Geophys. Res.*, *108*(D21), 8809, doi:10.1029/2002JD003093.

Thulasiraman, S., N. T. O'Neill, A. Royer, B. N. Holben, D. L. Westphal, and L. J. B. McArthur (2002), Sunphotometric observations of the 2001 Asian dust storm over Canada and the US, *Geophys. Res. Lett.*, *29*(8), 1255, doi:10.1029/2001GL014188.

Tyndall, G. S., R. A. Cox, C. Granier, R. Lesclaux, G. K. Moortgat, M. J. Pilling, A. R. Ravishankara, and T. J. Wallington (2001), Atmospheric

chemistry of small organic peroxy radicals, *J. Geophys. Res.*, *106*(D11), 12,157–12,182.

VanCuren, R. A. (2003), Asian aerosols in North America: Extracting the chemical composition and mass concentration of the Asian continental aerosol plume from long-term aerosol records in the western United States, *J. Geophys. Res.*, *108*(D20), 4623, doi:10.1029/2003JD003459.

VanCuren, R. A., and T. A. Cahill (2002), Asian aerosols in North America: Frequency and concentration of fine dust, *J. Geophys. Res.*, *107*(D24), 4804, doi:10.1029/2002JD002204.

Weber, R. J., D. Orsini, Y. Daun, Y. N. Lee, P. J. Klotz, and F. Brechtel (2001), A particle-into-liquid collector for rapid measurement of aerosol bulk chemical composition, *Aerosol Sci. Technol.*, *35*(3), 718–727.

Wesely, M. L. (1989), Parameterization of surface resistances to gaseous dry deposition in regional scale numerical models, *Atmos. Environ.*, *23*(6), 1293–1304.

Whittlestone, S., and W. Zahorowski (1998), Baseline radon detectors for shipboard use: Development and deployment in the First Aerosol Characterization Experiment (ACE 1), *J. Geophys. Res.*, *103*(D13), 16,743–16,751.

Wild, O., and H. Akimoto (2001), Intercontinental transport of ozone and its precursors in a three-dimensional global CTM, *J. Geophys. Res.*, *106*(D21), 27,729–27,744.

Yevich, R., and J. A. Logan (2003), An assessment of biofuel use and burning of agricultural waste in the developing world, *Global Biogeochem. Cycles*, *17*(4), 1095, doi:10.1029/2002GB001952.

Yienger, J. J., M. Galanter, T. A. Holloway, M. J. Phadnis, S. K. Guttikunda, G. R. Carmichael, W. J. Moxim, and H. Levy II (2000), The episodic nature of air pollution transport from Asia to North America, *J. Geophys. Res.*, *105*, 26,931–26,945.

Zhang, G. J., and N. A. McFarlane (1995), Sensitivity of climate simulations to the parameterization of cumulus convection in the Canadian Climate Center general circulation model, *Atmos. Ocean*, *33*(3), 407–446.

A. Clarke and S. Oltmans, National Oceanic and Atmospheric Administration, Aeronomy Laboratory, Boulder, CO 80309, USA.

O. Cooper, Cooperative Institute for Research in Environmental Sciences, University of Colorado, Boulder, CO 80309, USA.

A. H. Goldstein, M. McKay, and D. B. Millet, Department of Environmental Science, Policy, and Management, University of California, Berkeley, CA 94720, USA. (ahg@nature.berkeley.edu)

L. Horowitz, National Oceanic and Atmospheric Administration, Geophysical Fluid Dynamics Laboratory, Princeton, NJ 08542, USA.

R. Hudman and D. J. Jacob, Division of Engineering and Applied Sciences and Department of Earth and Planetary Sciences, Harvard University, Cambridge, MA 02138, USA.

L. Jaeglé, Department of Atmospheric Science, University of Washington, Seattle, WA 98195, USA.